Plasma Phys. Control. Fusion **54** (2012) 055008 (8pp) doi:10.1088/0741-3335/54/5/055008

Diffusive–convective transition for scrape-off layer transport and the heat-flux width

J R Myra, D A Russell and D A D'Ippolito

Lodestar Research Corp., 2400 Central Ave. P-5, Boulder, CO 80301, USA

Received 23 November 2011, in final form 16 March 2012
Published 12 April 2012
Online at stacks.iop.org/PPCF/54/055008

Abstract
Transport of plasma from the edge pedestal gradient region into the scrape-off layer (SOL) forms the heat exhaust channel. The properties of this channel are critical for future tokamak devices. The SOL heat-flux width is believed to be set by a competition between classical parallel transport and turbulent cross-field transport. In previous work, (Myra *et al* 2011 *J. Nucl. Mat.* **415** S605) focusing on modeling of the heat-flux width in the National Spherical Torus Experiment (NSTX), the possibility of a transition from quasi-diffusive to convective transport in the SOL was noticed. This transition, and the scaling of the heat-flux width, is explored here through additional SOL turbulence simulations using the SOLT code (Russell *et al* 2009 *Phys. Plasmas* **16** 122304). At the transition, the transport becomes intermittent, and the SOL width is broadened due to blob emission. Critical parameters for the transition are investigated, including the power flux into the SOL, the field line pitch, the connection length and the plasma collisionality. An inverse dependence of the heat-flux width on the poloidal field, also seen routinely in experiments, is noted and explained qualitatively.

(Some figures may appear in colour only in the online journal)

1. Introduction

In magnetically confined plasmas, the hot dense core region must transition to a colder plasma before interacting with material surfaces. This transition takes place in the edge and scrape-off-layer (SOL) regions. The SOL is the region of open field lines where plasma actually makes contact with material surfaces. This region is the main one of interest for this study. The edge is a somewhat poorly defined region which in present terminology will refer to the closed field line region just inside the separatrix or last-closed flux surface (LCFS). The difficulty in defining the edge region precisely reflects the coupling that exists between the core and the SOL, and the present lack of physics understanding of how this coupling works. From the point of view of SOL studies, the edge region is important as the source of SOL plasma, i.e. particles, energy and momentum transport across the LCFS to feed the SOL. Conversely, the plasma exhaust that leaves the tokamak through the SOL affects the density, temperature and flow profiles in the edge region.

The SOL and edge regions affect overall confinement of tokamak plasmas. Edge transport barriers give rise to enhanced confinement modes such as the high-confinement (H) -mode [1]. The transition from low- (L) mode to H-mode seems to be related to mean and/or oscillating (zonal) flows in the edge [2, 3]. Further evidence for the importance of the edge and SOL plasmas to tokamak operation comes from the beneficial effects on confinement resulting from lithium-coated plasma-facing surfaces [4, 5]. It is very important to understand the physics of the edge and SOL plasmas, both from the point of view of understanding core confinement, and mitigating potentially damaging interactions of plasma exhaust with material surfaces [6–8].

In the SOL itself, the simplest conceptual model is to regard the SOL plasma profiles as resulting from a competition between parallel and cross-field transport. This competition sets a characteristic SOL width [9, 10] which has been measured and fit to various (mostly diffusive cross-field) transport scalings [11, 12] motivated by theoretical considerations. While parallel transport is usually considered

 © 2012 IOP Publishing Ltd Printed in the UK & the USA

to be classical [13], often with flux limits and other corrections [14], cross-field transport is still more complex. Neoclassical effects on ion heat transport are believed to be important in some cases [12, 15, 16] but are beyond the scope of this study which focuses on the role of turbulence. In the far SOL, cross-field transport is usually dominated by turbulence-generated blob-filaments (often referred to as 'blobs') which are described in a number of review papers [17–19]. The motion of blobs is understood as being primarily convective. The physics of the near SOL (close to the LCFS) is more complicated. Here diffusive and convective processes can compete and the environment is typically more turbulent [20]. There is a strong need for reliable predictive models and corresponding experimental validation of plasma behavior in the near-SOL region.

The interactions of plasma exhaust with the surface of the divertor are a key motivation for understanding the near SOL [6, 7]. This topic has motivated a recent concerted effort on major tokamaks worldwide to measure the scaling of the SOL heat-flux width λ_q and peak power fluxes on the divertor [21–26]. This paper extends previous modeling work in this area. We begin, as a base case, with plasma conditions from the National Spherical Torus Experiment (NSTX) [27] for a case that was previously modeled [28, 29]. Starting from this base case, a number of numerical scaling experiments are carried out by varying code input parameters systematically one at a time. In addition to studying the dependence of λ_q on net power flux into the SOL, the field line pitch, the connection length and the plasma collisionality, we observe a transition in SOL dynamics from a nearly laminar, diffusive-like regime to a more turbulent convective transport regime. The properties of this diffusive–convective transition are a major focus of our paper.

This work is related to a few similar numerical studies in the literature. In particular, in a previous investigation [30] different confinement and transport states were identified in a two-dimensional (2D) resistive-g model depending on the strength of the turbulence drive. In [31] low- and high-confinement states of a simple magnetized torus were studied. The 2D model employed in these studies is similar to the model presented here. In another earlier approach, a simple one-dimensional model which allowed for competition between mode coupling and profile relaxation was shown to exhibit crossover from diffusive to ballistic turbulent transport governed by a single control parameter [32].

The formation of large-scale structures (including blobs [19], streamers and zonal flows [33]) from turbulence is a topic of considerable contemporary interest [34]. The edge and SOL parameter space is a very large one, and many different types of behaviors are observed and modeled. For example, in contrast to this study in an NSTX-like parameter regime, similar modeling efforts [35] of the heat-flux width and edge-SOL transport in the Alcator C-Mod tokamak [23] produced an entirely different phenomenon: quasi-coherent oscillations that appear to be a key controlling element of separatrix-crossing transport and blob formation in that case.

In section 2 the physics content of our numerical model and the procedure for our study are discussed. Results for the heat-flux width (λ_q) scaling and the diffusive–convective transition phenomena are given in section 3. Conclusions are presented in section 4.

2. Numerical model

2.1. Physics content

The physics model for this study is a three-field fluid turbulence model evolving density n, electron temperature $T_e \equiv T$, and electrostatic potential Φ. A simplified approach to the geometry is employed: turbulent structures are assumed to be constant filaments elongated in the direction of the background magnetic field $\boldsymbol{B}$. Thus, the dynamics is contained in the two dimensions perpendicular to $\boldsymbol{B}$. For tokamak plasmas, this plane is considered to be at the outboard midplane of the torus.

Computations are carried out with the 2D Scrape-Off-Layer Turbulence (SOLT) code [36]. Analytical closure relations are employed to describe the parallel dynamics. For example, the relationship of parallel current $J_\parallel$ to Φ is prescribed by a sheath closure on open field lines (generalized to allow for collision-dominated regimes), and a Wakatani–Hasegawa-like model [37] for $J_\parallel$ is employed on closed field lines to capture basic drift-wave physics.

The fundamental equations for the SOLT model are the vorticity, continuity and energy conservation (or alternatively temperature) equations:

$$\frac{\mathrm{d}}{\mathrm{d}t}\nabla\cdot n\nabla\Phi = A_{\mathrm{dw}}(\Phi, n) + \alpha_{\mathrm{sh}} J_\parallel - \beta\frac{\partial(nT)}{\partial y} \tag{1}$$

$$\frac{\mathrm{d}n}{\mathrm{d}t} = A_{\mathrm{dw}}(\Phi, n) - \alpha_{\mathrm{sh}}(nT^{1/2} - J_\parallel) \tag{2}$$

$$\frac{\mathrm{d}T}{\mathrm{d}t} = -\alpha_{\mathrm{sh}}\frac{q_\parallel}{n}. \tag{3}$$

Here we employ dimensionless notation (using the Bohm normalization with time-scale $\Omega_{\mathrm{ci}} = ZeB/m_{\mathrm{i}}c$ and space scale $\rho_{\mathrm{sr}} = c_{\mathrm{sr}}/\Omega_{\mathrm{ci}}$ where $c_{\mathrm{sr}}^2 = T_{\mathrm{er}}/m_{\mathrm{i}}$ and T_{er} is a reference temperature for the normalization). The simulation plane is denoted as the (x, y) plane where x is the radial direction and y is binormal (approximately poloidal). The radial variables r and x are used interchangeably in this paper; the only difference is that the origin of x is taken to be the LCFS. The convective derivative is written as $\mathrm{d}/\mathrm{d}t = \partial/\partial t + \boldsymbol{v}\cdot\nabla$ where $\boldsymbol{v} = \boldsymbol{e}_z \times \nabla\Phi$. A_{dw} is the drift-wave operator

$$A_{\mathrm{dw}}(\Phi, n) = \alpha_{\mathrm{dw}}\bar{T}^{3/2}\{\Phi - T\ln n\} \tag{4}$$

where for any quantity Q, $\langle Q\rangle \equiv \bar{Q}$ denotes the zonal or y average part and $\tilde{Q} \equiv \{Q\} \equiv Q - \bar{Q}$ denotes the fluctuating part. Thus A_{dw} enforces a Boltzmann response on fluctuations when the coefficient α_{dw} is large, in the spirit of the Wakatani–Hasegawa adiabaticity parameter. Note that the flux surface or y average of A_{dw} vanishes (as it must since it arises from $\nabla_\parallel J_\parallel$ on closed surfaces).

To close the system of equations, the parallel current and heat flux, $J_\parallel$, $q_\parallel$, must be expressed in terms of the dynamic variables Φ, n and T. A set of closure relations, valid for a range of collisionality regimes from conduction limited to sheath-connected, is employed here and discussed in detail in

appendix A of [29]. In particular, the parallel heat flux in the sheath-connected limit takes the form

$$q_{\|\mathrm{SL}} = s_{\mathrm{E}} n T^{3/2} \mathrm{e}^{(\Phi_{\mathrm{B}}-\Phi)/T} \tag{5}$$

where $\Phi_{\mathrm{B}} \sim 3\,\mathrm{T}$, and $s_{\mathrm{E}} \sim 6$ is the sheath energy transmission factor. In the collisional (conduction limited) case we have

$$q_{\|\mathrm{CL}} = \frac{3.2 n T^{3/2}}{\Lambda} \tag{6}$$

where the collisionality parameter Λ is defined below. A smooth interpolation between regimes is employed for intermediate cases.

The most important input parameters of the model for the present application are the sheath conductivity parameter

$$\alpha_{\mathrm{sh}} = \frac{\rho_{\mathrm{sr}}}{L_{\|}} \tag{7}$$

where $L_{\|}$ is the midplane-to-divertor-plate connection length in the SOL, the curvature drive parameter

$$\beta = \frac{2\rho_{\mathrm{sr}}}{R} \tag{8}$$

where R is the effective radius of curvature (approximately the major radius of the torus), and the collisionality parameter

$$\Lambda = \frac{\nu_{\mathrm{ei}} L_{\|}}{\Omega_{\mathrm{e}} \rho_{\mathrm{s}}} \tag{9}$$

which enters the closure relations for $J_{\|}$ and $q_{\|}$. Λ is related to the SOL electron parameter $\nu_{*\mathrm{e}}$ introduced by some authors as $\nu_{*\mathrm{e}} = L_{\|}/\lambda_{\mathrm{ei}} = \Lambda (m_{\mathrm{i}}/m_{\mathrm{e}})^{1/2}$, where λ_{ei} is the electron mean free path for collisions with ions.

The SOLT code solves the vorticity equation, by splitting equation (1) into zonally averaged and fluctuating parts. The zonally averaged part is manipulated into a conservative form for zonal (i.e. y) momentum conservation. The Boussinesq approximation is employed on the fluctuating part. Small diffusive terms are usually added to equations (1)–(3) to absorb high-wavenumber fluctuations before they cascade to the scale of the numerical grid. Further discussion of the SOLT model is given in previous publications [36, 40].

2.2. Procedure

In this work, our goal is to carry out a SOL simulation with as few artificial features as possible. The role of the edge region is to provide an effective boundary condition at the LCFS. Artificial source terms are added to equations (2) and (3) to maintain the time- and y-averaged n and T profiles *inside the LCFS* against losses to and in the SOL. These source functions are set to zero for $x > x_{\mathrm{s}} \approx -1$ cm so that the SOL is fueled entirely by transport across the LCFS, i.e. the SOL profiles themselves are determined self-consistently by the balance between perpendicular turbulent transport and parallel losses.

Following closely the procedure used in earlier work [29, 35], we impose a mean sheared flow velocity *in the edge region* to simulate the E_r well that is characteristic of H-mode plasmas

$$v_y = -E_x = -\frac{\tau}{n}\frac{\mathrm{d}}{\mathrm{d}x} n T_{\mathrm{e}}. \tag{10}$$

Setting $\tau = T_{\mathrm{i}}/T_{\mathrm{e}}$ forces balancing of the $\boldsymbol{E} \times \boldsymbol{B}$ and ion diamagnetic flow, which approximates the radial force balance characteristic of H-mode pedestals where the relatively flat core profiles transition sharply to their much smaller edge values. Here we regard τ as an order unity control parameter that regulates turbulence. Varying τ changes the power crossing the separatrix P_{sep}. In this way, we effectively achieve a heat flux-driven boundary condition for our SOL simulations. Results will be presented in this paper regarding P_{sep} as the independent variable.

It is important to recognize that the P_{sep} (i.e. τ) scans presented in this paper *hold the target edge profiles fixed*. (See figure 1.) Thus, qualitatively a P_{sep} scan can be regarded as a confinement scan: low P_{sep} (heat flux) and steep plasma profiles typical of H-mode imply good confinement, while high P_{sep} for the same profiles implies poorer confinement.

Our analysis begins with the plasma profiles and machine parameters of a particular discharge on NSTX that was modeled previously [29]. These parameters put our base case in a low collisionality sheath-connected regime. We then vary parameters about this real NSTX base case (keeping mean edge profiles for $x < x_{\mathrm{s}}$ fixed) to explore the parameter space of our numerical model. In particular we carry out τ scans for various values of $b_\theta = B_\theta/B$ (which specifies the field line pitch), SOL

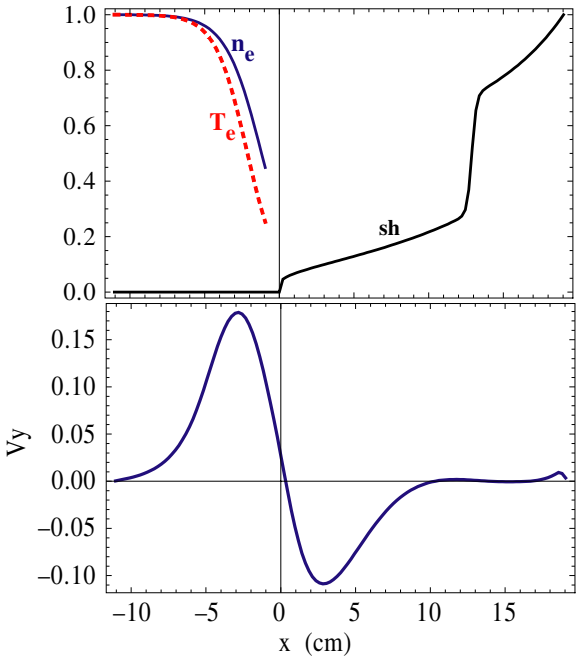

Figure 1. Upper panel: target plasma profiles in the edge, imposed for $x < -1$ cm, and radial variation of the sheath conductivity parameter α_{sh} in the SOL, $x > 0$. Here plasma profiles are normalized to their value at the left boundary and α_{sh} is normalized to its value at the right boundary. The sharp rise in α_{sh} at $x = 12$ is due to an imposed limiter. Lower panel: typical radial variation of the mean binormal flow velocity $\langle v_y \rangle$, imposed for $x < -1$ cm, but determined dynamically elsewhere. Noting that $E_r \sim -\langle v_y \rangle$ in our model, a typical E_r well exists just inside the separatrix.

connection length $L_\parallel$, and SOL collisionality Λ. For each run we calculate

$$P_{\rm sep} = 2\pi R b_\theta \int {\rm d}r\, q_\parallel \qquad (11)$$

where the $q_\parallel$ integral is over the entire SOL. The reference plasma parameters for the base case are $n_{\rm er} = 1.9 \times 10^{13}\,{\rm cm}^3$, $T_{\rm er} = 125\,{\rm eV}$, $B_{\rm r} = 0.27\,{\rm T}$ (outboard midplane) yielding $\rho_{\rm sr} = 0.60\,{\rm cm}$, $\Omega_{\rm ir} = 1.29 \times 10^7\,{\rm s}^{-1}$, $c_{\rm sr} = 7.74 \times 10^6\,{\rm cm\,s}^{-1}$. The reference values of density and temperature are taken at the inflection point of the tanh-function fits. (See figure 1). Other inputs are $R = 150\,{\rm cm}$, deuterium plasma (charge $Z = 1$, mass $A = 2$) and $b_\theta = 0.3$ (outboard midplane). Dimensionless SOLT input parameters are $\beta = 8.0 \times 10^{-3}$, $\mu = 0.1$ (dimensionless viscosity), $D = 0.01$ (dimensionless density diffusion). The sheath conductivity is $\alpha_{\rm sh} = \rho_{\rm sr}/(a_{\rm f} + b_{\rm f}\ln[x({\rm cm})])$ where the connection length $L_\parallel$ in the denominator was fit from an equilibrium reconstruction with $a_{\rm f} = 750\,{\rm cm}$ and $b_{\rm f} = -225\,{\rm cm}$. The adiabaticity parameter on the core-side boundary is $\alpha_{\rm dw} = 0.172$, estimated from NSTX parameters, and its tanh-shaped profile goes to zero at the LCFS. Experimentally, the value $P_{\rm sep} = 0.8\,{\rm MW}$ was observed for this discharge.

3. Results

Experiments have revealed a consistent inverse dependence of the heat-flux width on the plasma current $I_{\rm p} \propto B_\theta$ and relatively less dependence on other parameters for a given tokamak. This observation motivates a theoretical study of the heat-flux width scaling, and the choice of parameter scans studied in section 3.1. It will be seen that while qualitative scalings pertain, there is no one power-law scaling that describes all regimes. Rather, we find the interesting result that there is a break in scaling that separates two regimes for the SOL, a somewhat laminar diffusive-like regime, and a turbulent blob-dominated regime. These regimes are investigated further in section 3.2.

3.1. Heat-flux width scaling

In the following, results are presented for the heat-flux width in $P_{\rm sep}$ scans using the base case parameters and then for separate scans in which b_θ, $L_\parallel$ and Λ are modified by specified amounts. For these heat-flux width scaling studies, we employ an integral definition [38] of λ_q based on equation (9)

$$\lambda_q = \frac{P_{\rm sep}}{2\pi R b_\theta q_{\parallel{\rm peak}}} \qquad (12)$$

where $q_{\parallel{\rm peak}}$ is the peak value of the heat flux, obtained at the first grid-point in the SOL.

Figure 2 shows the results of a study in which b_θ is varied, with the base case denoted by $b_{\theta 0}$. The parameter b_θ enters the simulation inputs in two ways: (i) it appears explicitly in equation (11) for $P_{\rm sep}$, and (ii) it affects the connection length $L_\parallel$ which, for a given flux surface shape, changes with the field line pitch.

As illustrated in figure 2, there is a consistent inverse dependence of λ_q on b_θ which for low powers can be approximated as $\lambda_q \propto 1/b_\theta^m$ with $m \sim 0.5$ at low power but closer to 1 at high power. This inverse dependence is qualitatively similar to the inverse dependence of λ_q on the plasma current $I_{\rm p}$ that has been noted in several experiments [21–23]. Our previous modeling work [29] on specific experimental shot sequences also showed this trend.

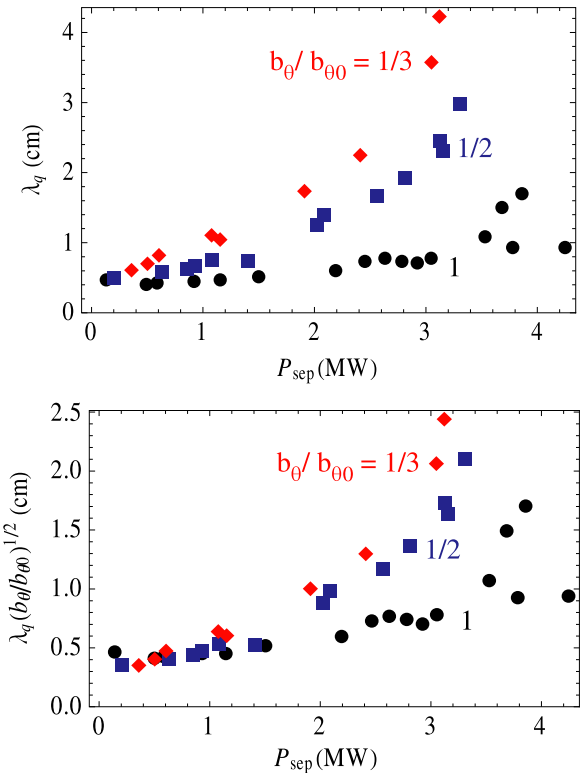

Figure 2. Upper panel: power variation of the heat-flux width for various field line angles: base case with $b_\theta \equiv b_{\theta 0} = 0.3$ (black disks), $b_\theta/b_{\theta 0} = 1/2$ (blue squares) and $b_\theta/b_{\theta 0} = 1/3$ (red diamonds). There is a consistent inverse dependence on b_θ. Lower panel: same data with $(b_{\theta 0}/b_\theta)^{1/2}$ scaling removed. At low powers $P < 2\,{\rm MW}$, this scaling unifies the results; however, at high powers the b_θ dependence is stronger.

We can understand this dependence from equation (11). If b_θ is decreased at constant $P_{\rm sep}$, then the integral of $q_\parallel$ must rise. From equation (5) this can only happen if density and temperature at the separatrix rise and/or if the SOL width increases. Both effects occur, and both require stronger levels of turbulence carrying plasma from the edge region into the SOL.

It is interesting that at $P_{\rm sep} \sim 2\,{\rm MW}$ there is a break from the low-power $\lambda_q \propto 1/b_\theta^{1/2}$ scaling. This break in scaling turns out to be related to the diffusive–convective transition that is the second subject of this paper.

Although the connection length $L_\parallel$ changes when b_θ is changed, further numerical experimentation reveals that $L_\parallel$ itself is not the main contributor to the b_θ scaling of figure 2. In figure 3 the connection length was artificially varied by changing $\alpha_{\rm sh}$ while holding b_θ fixed. Little explicit dependence resulted. This result is qualitatively consistent with observations on Alcator C-Mod that showed λ_q to be insensitive to $L_\parallel$ in experiments that compared single and double null SOL geometries. This result is not

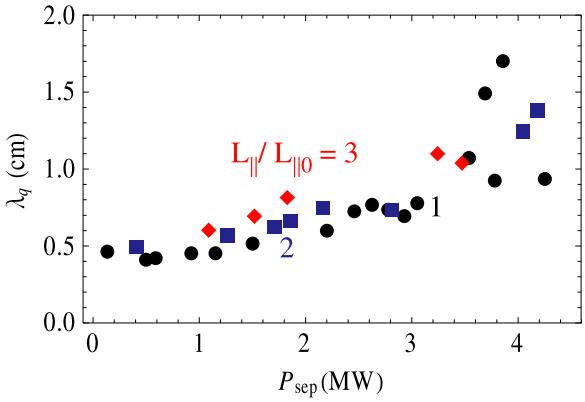

Figure 3. Power variation of the heat-flux width for various connection lengths: base case (black disks), $L_\parallel/L_{\parallel 0} = 2$ (blue squares) and $L_\parallel/L_{\parallel 0} = 3$ (red diamonds). There is little explicit dependence on the connection length.

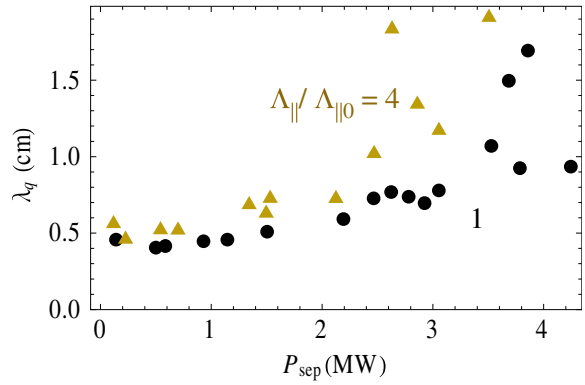

Figure 4. Power variation of the heat-flux width for various collisionalities: base case (black disks), $\Lambda/\Lambda 0 = 4$ (gold triangles). There is a weak, but consistent increase of λ_q with collisionality.

unexpected from equations (5) and (11), which have no explicit $L_\parallel$ dependence in the sheath-connected regime which characterizes the base case. The connection length does enter Λ in the conduction limited regime of equation (6). This motivated the next numerical experiment.

In figure 4, b_θ and $L_\parallel$ (i.e. α_{sh}) were held fixed, but the collisionality parameter Λ was artificially multiplied by a constant factor in one of the scans. A weak increase in λ_q with Λ is evident. The dependence is stronger at higher P_{sep}, as was also the case in the b_θ study of figure 2. An increase in the SOL density width with collisionality for blob-driven transport has been previously noted in experiments [39] and simulations [39, 40] where it is related to an increase of blob speed [41]. The collisionality dependence of λ_q seen here can be understood qualitatively by an argument similar to that given for the b_θ dependence. From equations (6) and (11), if Λ is increased at constant P_{sep} then either n and T must go up at the separatrix, and/or the SOL must broaden to compensate. Both effects occur, and both require stronger levels of turbulence carrying plasma from the edge region into the SOL.

3.2. Diffusive–convective transition

As evidenced from the scans in the preceding section, at a given P_{sep} the SOL width broadens with decreasing b_θ, and

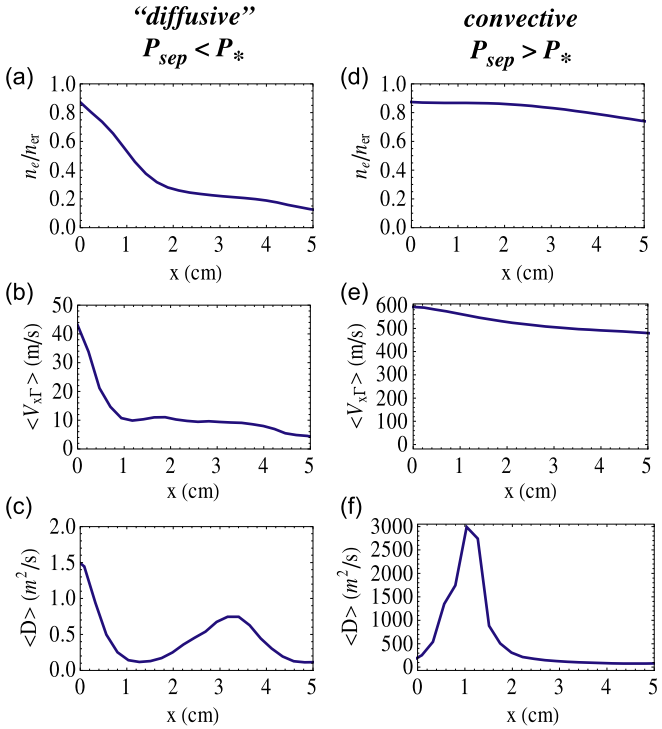

Figure 5. Profile comparisons in the SOL contrasting the low-power quasi-diffusive regime (left column) and the high-power convective regime (right column). Shown are density profiles in (*a*) and (*d*), effective radial convection velocity in (*b*) and (*e*), and effective diffusion coefficient in (c) and (*f*). Note the flattening of the density and velocity profiles in the convective regime, (*d*) and (*e*).

increasing collisionality Λ. The mechanism for the broadening of the SOL width is increased cross-field turbulent transport. In analogy with critical Reynolds number phenomena in neutral fluid turbulence, the turbulence and cross-field transport in the present system appear to undergo a qualitative change from a nearly laminar diffusive-like regime to a turbulent convective regime which tends to be dominated by blob ejection.

Figure 5 shows plasma profile comparisons in the SOL contrasting the low-power quasi-diffusive regime and the high-power convective regime. The cases correspond to $P_{sep} = 0.6$ MW and 3.9 MW respectively, with $b_\theta/b_{\theta 0} = 1/2$, $\bar{\mu} = 0.01$ and $D = 0$. We choose reduced *ad hoc* diffusion and viscosity parameters here and for figure 6 so as not to bias the characterization of the diffusive regime. (Smaller time steps are required with these choices, so they are not employed for the broad parameter studies of the previous section.) The low-power regime is not strictly diffusive because there is no separation of scales (i.e. there is no step size that is small-scale with respect to the profiles). Nevertheless, an effective diffusion coefficient can be defined as $D_{eff} = \Gamma/\nabla\langle n\rangle$ where $\Gamma = \langle n v_x\rangle$ is the particle flux. The fact that D_{eff} varies on a scale similar to that of $\langle n\rangle$ itself suggests the absence of a truly diffusive process. It is also possible to define an effective radial convection velocity $V_{eff} = \Gamma/\langle n\rangle$. In the high-power regime, $P > P_*$ (where $P_* \sim 2$ MW from figures 2 and 4), $\langle n\rangle$ and V_{eff} are noticeably flattened, and V_{eff} appears to be a better descriptor of transport than the wildly varying D_{eff}.

Further evidence for a change of character in the transport comes from examining the probability distribution functions

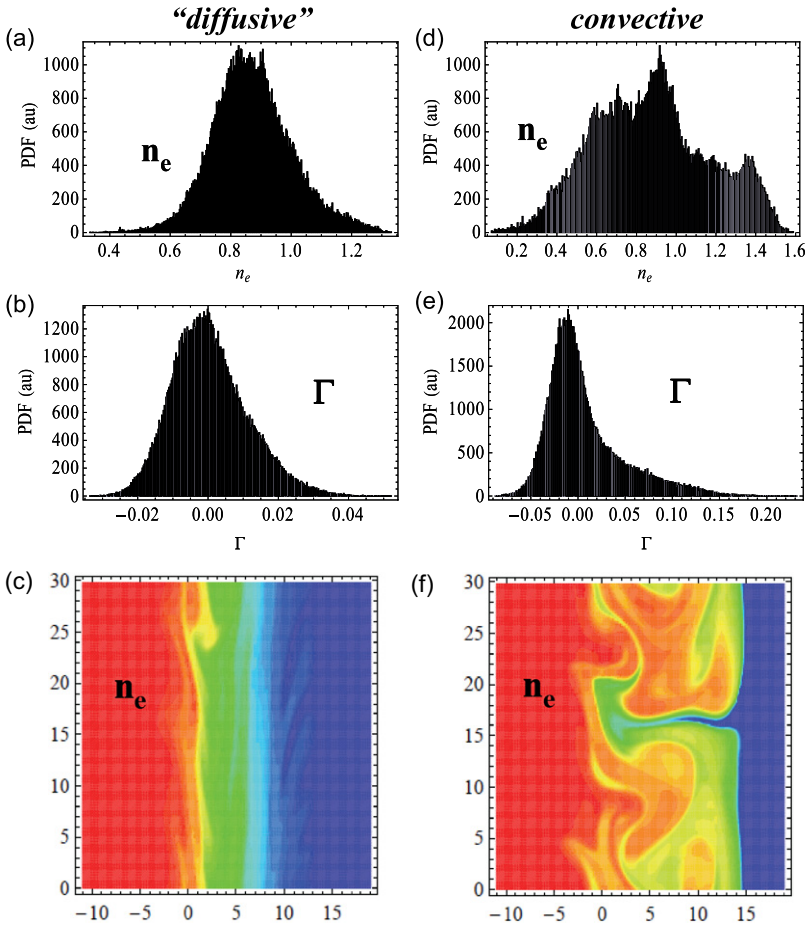

Figure 6. PDFs contrasting the low-power 'diffusive' regime and the high-power convective regime. Show are the PDFs of density in (*a*) and (*d*), and particle flux in (*b*) and (*e*) The scale of the flux in (*e*) is about 5 times larger than in (*b*) due to the much faster transport. Two-dimensional snap-shots in the (x, y) plane of the density (color palette, log scale) in (*c*) and (*f*) illustrate the transition from nearly laminar to strongly turbulent dynamics. The high-density core plasma is to the left.

(PDFs) of density and flux variations shown in figure 6 for the same two extreme cases. Note also the transition from nearly laminar to strongly turbulent dynamics in going from the low-power 'diffusive' case to the high-power convective case.

The presence of convective transport and strong PDF tails for the high-power case shown in figures 5 and 6 is usually indicative of blob formation and ejection, and also manifests itself in the time history of synthetic probe diagnostics in SOLT. Time traces of the density in the SOL are shown in figure 7(*a*) comparing a low-power ($P_{\rm sep} = 1.1\,$MW) and a high-power ($P_{\rm sep} = 3.3\,$MW) case, from the $b_\theta/b_{\theta 0} = 1/2$ scan of figure 2. The bursts seen in the high-power case are usually accompanied by blob ejection. A particularly good example of this is shown in figure 7(*b*).

So far we have seen evidence for a diffusive–convective transition from rather extreme cases, chosen to highlight the differences. In fact, for most of the runs, the transition, while qualitative, is rather easily identified by visual inspection of the $V_{\rm eff}$ profiles and snap-shots of the dynamics. Before attempting to identify more quantitatively the critical parameters for the transition, it is useful to examine heuristic scalings for diffusive and convective transport.

For turbulent diffusive transport, we expect a mixing-length scaling to hold, where we can estimate $D_{\rm eff} \sim \gamma/k_y^2$ with γ a characteristic growth rate of instabilities sustained by the time-averaged profiles, and k_y a characteristic wavenumber. A characteristic velocity in the diffusive regime is therefore $D_{\rm eff}/\lambda_q$ where we take λ_q as the typical profile scale.

For blob-dominated convective transport, we can estimate the characteristic net convective velocity as $v_{\rm b} f_{\rm p}$ where $v_{\rm b}$ is the radial velocity of an individual blob and $f_{\rm p}$ is the blob packing fraction (the percentage of space occupied by blobs). Furthermore, using the blob correspondence principle [17, 19] we estimate $v_{\rm b} \sim \gamma/k_y$. Thus

$$V_{\rm eff} \sim \begin{cases} D_{\rm eff}\nabla \ln q_\parallel \sim \frac{\gamma}{k_y^2 \lambda_q} & \text{diffusive} \\ v_{\rm b} f_{\rm p} \sim \frac{\gamma}{k_y} f_{\rm p} & \text{convective.} \end{cases} \tag{13}$$

Comparing the estimates for $V_{\rm eff}$ with diffusive and convective transport mechanisms we find the ratio

$$\text{diffusion} : \text{convection} = \frac{1}{k_y \lambda_q} : f_{\rm p}. \tag{14}$$

This leads to the following scenario. At sufficiently low $P_{\rm sep}$ where λ_q and hence $k_y\lambda_q$ are small, diffusion dominates convection. As $P_{\rm sep}$ is raised, we find numerically that both k_y and λ_q increase; thus there is a decrease in $1/(k_y\lambda_q)$.

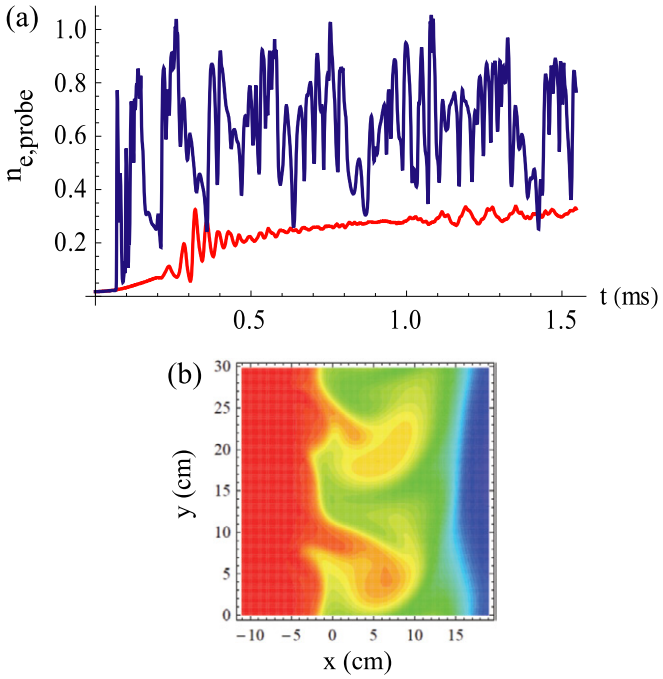

Figure 7. (*a*) Time histories of the fluctuating density in the SOL for a high-power turbulent convective case (upper blue trace), and a low-power nearly laminar diffusive case (lower red trace). The bursty character of the signal is evident in the convective case. The bursts are often associated with the emission of one or more blobs. (*b*) Two-dimensional snapshot in the (x, y) plane of the density (color palette, log scale) at a time corresponding to a strong burst and emission of two blobs in the turbulent convective case. The high density core plasma is to the left.

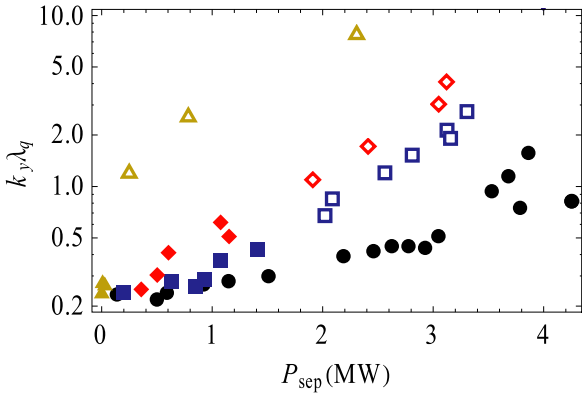

Figure 8. Power scaling of the heat-flux width normalized to the mean turbulent wavenumber, k_y. The four cases are the base case with $b_\theta \equiv b_{\theta 0} = 0.3$ (black disks), $b_\theta/b_{\theta 0} = 1/2$ (blue squares), $b_\theta/b_{\theta 0} = 1/3$ (red diamonds) and $b_\theta/b_{\theta 0} = 1/2$, $\Lambda_\parallel/\Lambda_{\parallel 0} = 16$ (gold triangles). Filled (open) symbols indicate the diffusive (convective) regime. The transition occurs at $k_y\lambda_q \sim 1$.

For sufficiently large λ_q, i.e. with flattened profiles, diffusion cannot supply enough flux to deliver the power through the SOL. At this point the system responds by starting to eject more and more blobs, i.e. increasing the packing fraction f_p. Therefore, we expect the diffusive–convective transition to occur for $k_y\lambda_q$ of order unity.

Figure 8 combines the data for four scans. Three of the scans are the same b_θ cases considered in figure 2. The fourth case is an extreme collisionality case ($b_\theta/b_{\theta 0} = 1/2$ and $\Lambda/\Lambda_0 = 16$) chosen to provide data in the small P_{sep} large $k_y\lambda_q$ portion of the space. In this figure, open symbols indicate cases in the convective regime. There is good qualitative agreement with the heuristic prediction that the convective regime occupies the region $k_y\lambda_q > 1$.

4. Discussion and conclusions

Using SOLT code simulations, with fixed edge profiles, we have shown that SOL cross-field transport depends on the net power flux into the SOL, P_{sep}, the normalized poloidal magnetic field b_θ, the SOL connection length $L_\parallel$ and the plasma collisionality Λ. Below some critical power level, $P_{sep} < P_*$, the near-SOL cross-field transport is quasi-diffusive; whereas for $P_{sep} > P_*$ the SOL makes a transition into a convective blob-dominated regime.

The critical power P_* depends on b_θ and Λ. As can be seen from figure 8, P_* increases with b_θ and decreases with Λ. One way of characterizing the critical parameters for the transition is that the convective, blob-dominated regime occurs for $k_y\lambda_q > 1$ where k_y is a characteristic poloidal wavenumber. The parallel heat-flux width λ_q also scales with poloidal magnetic field and collisionality. We find that $\lambda_q \sim b_\theta^{-m}$ with $m \sim 0.5$ in the diffusive regime and $m \sim 1$ in the convective regime.

A general trend emerging from the recent worldwide tokamak data [21–26] on the scaling of λ_q is an inverse dependence on plasma current I_p for fixed machine size (a, R), or equivalently in terms of toroidal field B_t and safety factor q, a positive scaling with q and an inverse scaling with B_t. In this respect, the present results are qualitatively in accord with the experimental scalings. From collisionality scaling studies, we find λ_q increases with Λ, but is nearly independent of the SOL connection length $L_\parallel$ in the sheath-connected regime. This lack of explicit $L_\parallel$ dependence is qualitatively consistent with experiments on Alcator C-Mod.

In interpreting the results in this paper, it is important to recall that our P_{sep} scans hold edge (i.e. closed surface) profiles fixed. Therefore, in some sense, one can say that the low P_{sep} more laminar cases correspond to better edge confinement than the high P_{sep} convective blob-dominated cases. A similar trend for blob emission was noted in experiments on NSTX [42]. The relation of confinement to the SOL width for Alcator C-Mod was emphasized in [23].

Fully predictive calculations of λ_q and direct comparisons of the same with experimental scalings are not yet possible and will require coupling to models for edge profiles, and hence transport, in the pedestal and core regions. Other SOL modeling work [29, 35] has employed the alternative strategy of using experimentally measured edge profiles for each P_{sep} to obtain a *net* power scaling of the SOL width. These studies have found only a weak net dependence on power, not inconsistent with recent experimental work [23, 26].

The present model is rudimentary in many respects, such as its use of 2D geometry and reduced physics. Nevertheless, it is hoped that the observations presented here will further experimental, theoretical and numerical enquiries leading to the development of a fully predictive theory for the SOL heat-flux width and SOL dynamics in tokamak plasmas.

Acknowledgments

This work was motivated in part by previous modeling [28, 29] of data from the NSTX experiment. The authors wish to thank their colleagues J-W Ahn, J Boedo, D P Lundberg, R Maingi, R J Maqueda, D P Stotler, M Umansky and S J Zweben for stimulating discussions of NSTX scrape-off-layer physics and for providing characteristic data for the starting point of these studies. This work was supported by the US Department of Energy (DOE) under grants DE-FG02-97ER54392 and DE-FG02-02ER54678; however, such support does not constitute an endorsement by the DOE of the views expressed herein.

References

[1] Wagner F *et al* 1982 *Phys. Rev. Lett.* **49** 1408
[2] Zweben S J *et al* 2010 *Phys. Plasmas* **17** 102502
[3] Conway G D, Angioni C, Ryter F, Sauter P, Vicente J and ASDEX Upgrade Team 2011 *Phys. Rev. Lett.* **106** 065001
[4] Canik J M *et al* 2011 *Phys. Plasmas* **18** 056118
[5] Maingi R *et al* 2009 *Phys. Rev. Lett.* **103** 075001
[6] Lipschultz B *et al* 2007 *Nucl. Fusion* **47** 1189
[7] Herrmann A 2002 *Plasma Phys. Control. Fusion* **44** 883
[8] Loarte A *et al* 2007 *Nucl. Fusion* **47** S203
[9] Counsell G F, Connor J W, Erents S K, Field A R, Fielding S J, LaBombard B and Morel K M 1999 *J. Nucl. Mater.* **266–269** 91
[10] Itoh S-I and Itoh K 1994 *Plasma Phys. Control. Fusion* **36** 1845
[11] Ahn J-W, Counsell G F and Kirk A 2006 *Plasma Phys. Control. Fusion* **48** 1077
[12] Fundamenski W *et al* 2005 *Nucl. Fusion* **45** 950
[13] Braginskii S I 1965 Transport processes in a plasma *Reviews of Plasma Physics* vol 1 (New York: Consultants Bureau)
[14] Stangeby P C, Canik J M and Whyte D G 2010 *Nucl. Fusion* **50** 125003
[15] Goldston R J 2012 *Nucl. Fusion* **52** 013009
[16] Cummings J, Chang C S, Park G and Pankin A 2010 *Bull. Am. Phys. Soc.* **55** 279
[17] Krasheninnikov S I, D'Ippolito D A and Myra J R 2008 *J. Plasma Phys.* **74** 679
[18] Garcia O E 2009 *Plasma Fusion Res.* **4** 019
[19] D'Ippolito D A, Myra J R and Zweben S J 2011 *Phys. Plasmas* **18** 060501
[20] Zweben S J *et al* 2007 *Plasma Phys. Control. Fusion* **49** S1
[21] Lasnier C J *et al* 2011 *J. Nucl. Mater.* **415** S353
[22] Gray T K, Maingi R, Soukhanovskii V A, Surany J E, Ahn J-W and McLean A G 2011 *J Nucl. Mater.* **415** S360
[23] LaBombard B *et al* 2011 *Phys. Plasmas* **18** 056104
[24] Fundamenski W *et al* 2011 *Nucl. Fusion* **51** 083028
[25] Eich T *et al* 2011 *J. Nucl. Mater.* **415** S856
[26] Eich T *et al* 2011 *Phys. Rev. Lett.* **107** 215001
[27] Kaye S M *et al* 2001 *Phys. Plasmas* **8** 1977
[28] Myra J R, Russell D A, D'Ippolito D A, Ahn J-W, Maingi R, Maqueda R J, Lundberg D P, Stotler D P, Zweben S J and Umansky M 2011 *J. Nucl. Mater.* **415** S605
[29] Myra J R *et al* 2011 *Phys. Plasmas* **18** 012305
[30] Garcia O E, Bian N H, Paulsen J-V, Benkadda S and Rypdal K 2003 *Plasma Phys. Control. Fusion* **45** 919
[31] Ricci P, Rogers B N and Brunner S 2008 *Phys. Rev. Lett.* **100** 225002
[32] Sarazin Y, Garbet X, Ghendrih Ph and Benkadda S 2000 *Phys. Plasmas* **7** 1085
[33] Diamond P H, Itoh S-I, Itoh K and Hahm T S 2005 *Plasma Phys. Control. Fusion* **47** R35
[34] Benkadda S, Klochkov D N, Popel S I and Izvekova Yu N 2011 *Phys. Plasmas* **18** 052306
[35] Russell D A *et al* 2011 *Bull. Am. Phys. Soc.* **56** 140
[36] Russell D A, Myra J R and D'Ippolito D A 2009 *Phys. Plasmas* **16** 122304
[37] Wakatani M and Hasegawa A 1984 *Phys. Fluids* **27** 611
[38] Loarte A *et al* 1999 *J. Nucl. Mater.* **266–269** 587
[39] Garcia O E, Horacek J, Pitts R A, Nielsen A H, Fundamenski W, Naulin V and Rasmussen J J 2007 *Nucl. Fusion* **47** 667
[40] Russell D A, Myra J R and D'Ippolito D A 2007 *Phys. Plasmas* **14** 102307
[41] Myra J R, Russell D A and D'Ippolito D A 2006 *Phys. Plasmas* **13** 112502
[42] Agostini M, Zweben S J, Cavazzana R, Scarin P, Serianni G, Maqueda R J and Stotler D P 2007 *Phys. Plasmas* **14** 102305